

# First-principles study of the thermoelectric properties of strained graphene nanoribbons

Pei Shan Emmeline Yeo,<sup>1,2</sup> Michael B. Sullivan,<sup>1</sup> Kian Ping Loh,<sup>2</sup> and Chee Kwan Gan<sup>1,\*</sup>

<sup>1</sup>*Institute of High Performance Computing, Agency for Science, Technology and Research, 1 Fusionopolis Way, #16-16 Connexis, Singapore 138632*

<sup>2</sup>*Department of Chemistry, National University of Singapore, 3 Science Drive 3, Singapore 117543*

We study the transport properties, in particular, the thermoelectric figure of merit ( $ZT$ ) of armchair graphene nanoribbons, AGNR- $N$  (for  $N = 4 - 12$ , with widths ranging from 3.7 to 13.6 Å) through strain engineering, where  $N$  is the number of carbon dimer lines across the AGNR width. We find that the tensile strain applied to AGNR- $N$  changes the transport properties by modifying the electronic structures and phonon dispersion relations. The tensile strain increases the  $ZT$  value of the AGNR- $N$  families with  $N = 3p$  and  $N = 3p + 2$ , where  $p$  is an integer. Our analysis based on accurate density-functional theory calculations suggests a possible route to increase the  $ZT$  values of AGNR- $N$  for potential thermoelectric applications.

PACS numbers:

Keywords:

## I. INTRODUCTION

Currently thermoelectric materials receive considerable attention<sup>1</sup> due to their ability to produce electricity from waste heat generated in, for example, power plants and refrigeration units. The efficiency of a thermoelectric material is characterized by the figure of merit

$$ZT = \frac{G_e S^2}{K_e + K_{ph}} T$$

where  $G_e$  is the electrical conductance,  $S$  is the Seebeck coefficient,  $K_e$  ( $K_{ph}$ ) is the thermal conductance due to electrons (phonons), and  $T$  is the absolute temperature. It is challenging to engineer thermoelectric materials because the parameters  $G_e$ ,  $S$ ,  $K_e$ , and  $K_{ph}$  are intricately interrelated; an attempt to improve one parameter usually detrimentally affects the others.<sup>2</sup> It is generally agreed that for thermoelectric generators to be viable, a material with  $ZT \sim 2 - 4$  is required.<sup>3,4</sup>

Current state-of-the-art thermoelectric materials<sup>4-7</sup> such as single-layer  $\text{Bi}_2\text{Te}_3$  and  $\text{AgPb}_{18}\text{SbTe}_{20}$  possess  $ZT$  between 2 and 3, but they are composed of high atomic number elements, thus making them both expensive and heavy. Graphene, which is composed of a hexagonal network of lightweight carbon atoms, with extremely high electron mobility and long electron mean free paths,<sup>8</sup> is a potential thermoelectric material. Experimental measurements of  $S$  for graphene showed values of  $80 \mu\text{VK}^{-1}$  at 300 K,<sup>9</sup>  $39 \mu\text{VK}^{-1}$  at 255 K,<sup>10</sup> and  $100 \mu\text{VK}^{-1}$  at 280 K,<sup>11</sup> which are moderate compared to  $150 - 850 \mu\text{VK}^{-1}$  at room temperature for the inorganic materials,<sup>12-14</sup> but comparable to other organic thermoelectric materials such as conducting polymers.<sup>15</sup>

Since graphene has very high  $K_{ph}$ ,<sup>16-19</sup> a common approach to increase  $ZT$  of graphene-related materials is to reduce  $K_{ph}$ . For example, edge disorder decreases the phonon mean free path and therefore reduces  $K_{ph}$ , which may increase  $ZT$ . However, edge disorder impacts the

electronic structure of the materials as well. In the case of armchair graphene nanoribbons (GNRs),<sup>20,21</sup> edge disorder turns out to be detrimental to  $ZT$ ; whereas for zigzag graphene nanoribbons, a high  $ZT \sim 4$  was obtained.<sup>22</sup>

Introducing vacancies into GNRs may also reduce phonon thermal conductance. Randomly distributed vacancies tend to decrease  $ZT$ ,<sup>20,21</sup> while periodically distributed lattice defects increases  $ZT$ . The maximal  $ZT$  attainable<sup>23,24</sup> is  $\sim 0.2$  to  $0.3$ .

Other methods to suppress  $K_{ph}$  involves crafting graphene into novel nanostructures. Graphene nanojunctions, which consist of graphene domains with different widths connected together,<sup>25</sup> demonstrated a maximum  $ZT \sim 0.6$ . In a similar vein, attaching “stub” structures to the edges of GNRs<sup>26</sup> resulted in  $ZT \sim 0.25$ . In the case of kinked GNRs, a maximum  $ZT \sim 0.4$  can be achieved.<sup>27</sup> Cutting graphene into “nanowiggles”<sup>28</sup> delivered a maximum  $ZT \sim 0.79$ , while crafting graphene into structures with alternating armchair-edge and zigzag-edge domains<sup>29</sup> delivered  $ZT \sim 1$ .

There have also been attempts to combine the two methods above by etching periodic vacancies into novel graphene nanostructures. A maximum  $ZT$  of 0.4 and even 5 have been reported in these structures.<sup>21,30</sup>

Finally, the thermoelectric properties of graphene may be improved by incorporating heteroatoms<sup>31,32</sup> or isotopes<sup>33,34</sup> into it. For example, by attaching hydrogen atoms on the surface of the GNRs,  $ZT \sim 26$  was reported.<sup>31</sup> The thermoelectric properties of hybrid nanoribbons consisting of alternating graphene and hexagonal boron nitride regions have also been investigated.<sup>32</sup> A maximum  $ZT \sim 0.7$  was observed.

The strategies mentioned above face several challenges as they involve engineering complex shapes out of GNRs. Furthermore, foreign entities incorporated into graphene are either removed,<sup>35</sup> or nucleate to form large clusters,<sup>36</sup> when subjected to elevated temperatures. Inspired by previous works that showed that tensile strain reduces the  $K_{ph}$  of graphene-related materials,<sup>37-39</sup> we examine

the effect of strain on the  $ZT$  value of armchair graphene nanoribbons (AGNRs). Compared to the methods mentioned above, tensile strain<sup>40</sup> is relatively easier to be imposed on AGNRs, thus enabling a possible route to manipulate the  $ZT$  values.

## II. METHODOLOGY

To calculate the thermoelectric properties of the AGNR- $N$  with a strain parameter  $\varepsilon$ , we use the Landauer approach to calculate the transport properties, where the electrical conductance  $G_e$ , the Seebeck coefficient  $S$ , and the thermal conductance due to electrons  $K_e$  are obtained in the linear response regime under an open circuit condition:

$$G_e(\varepsilon, T) = e^2 L_0, \quad (1)$$

$$S(\varepsilon, T) = -\frac{1}{eT} \frac{L_1}{L_0}, \quad (2)$$

$$K_e(\varepsilon, T) = \frac{1}{T} \left( L_2 - \frac{L_1^2}{L_0} \right), \quad (3)$$

where the  $n$ th order Lorenz function is given by

$$L_n = \frac{2}{h} \int_{-\infty}^{\infty} \theta_e(E) (E - \mu)^n \left( -\frac{\partial f(E, \mu, T)}{\partial E} \right) dE. \quad (4)$$

In the above equations,  $e$  is the elementary charge,  $f(E, \mu, T) = [e^{(E-\mu)/kT} + 1]^{-1}$  is the Fermi-Dirac distribution with energy  $E$ , chemical potential  $\mu$ , and temperature  $T$ . The Planck and Boltzmann constants are  $h$  and  $k$ , respectively.  $\theta_e(E)$  is the electronic transmission function, which is the number of effective modes available for electronic transport at  $E$ . We expect Eq. 1 to Eq. 4 to be valid even for the case of one-atom thick AGNRs since the approximations made to derive them do not take the dimensionality of the system into account. Assuming ballistic transport (since our system sizes are much smaller than the typical electron<sup>41</sup> and phonon<sup>42</sup> mean free paths) and completely uniform contact and transport regions, we can calculate  $\theta_e(E)$  by counting the number of bands at  $E$  from the electronic band structure along the transport direction of interest.<sup>43,44</sup> We note here that for more general cases,  $\theta_e(E)$  may be calculated using the nonequilibrium Green's function method.<sup>45</sup> Since the highest doping concentration achievable<sup>46</sup> so far by molecular charge-transfer and hetero-atom doping of graphene is  $\sim 10^{13} \text{ cm}^{-2}$ , we investigate doping concentrations in AGNR- $N$  from  $-10^{14}$  to  $10^{14} \text{ cm}^{-2}$ ; with a negative (positive) concentration representing electron or n-type doping (hole or p-type doping). We consider both

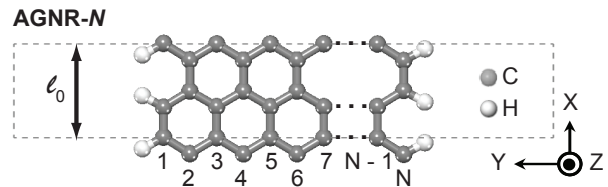


FIG. 1: The unit cell of AGNR- $N$ , with optimized length  $\ell_0$ . The dashed grey lines denote the boundaries of the unit cell.

n- and p-type doping because thermoelectric devices requires both types of materials. We restrict our study to temperatures from 200 to 800 K.

We perform nonspin-polarized density-functional theory (DFT) calculations on AGNRs using the SIESTA package.<sup>47</sup> The unit cell of AGNR- $N$  is shown in Figure 1, where  $N$  is the number of carbon dimer lines across the AGNR, and each carbon atom at the edge is terminated with a single hydrogen atom. A vacuum separation of at least  $15 \text{ \AA}$  is imposed in the  $y$  and  $z$  directions, where we use the convention adopted in Figure 1. The local density approximation (LDA) is used for the exchange-correlation functional. Troullier-Martins pseudopotentials and double- $\zeta$  basis sets are used for the carbon and hydrogen atoms. A mesh cutoff of 400 Ryd is used. We obtain the optimized length  $\ell_0$  of each  $N$  in the  $x$  direction (i.e., the transport direction) by relaxing the atomic positions of AGNR- $N$  with different ribbon lengths  $\ell$ . The atomic relaxation is performed using the conjugate gradient algorithm with a force tolerance criterion of  $10^{-3} \text{ eV/\AA}$ . The total energies of the relaxed structures are fitted to a polynomial function as a function of  $\ell$  to obtain  $\ell_0$ . For the strained AGNRs, we use unit cells with  $\ell = (1 + \varepsilon)\ell_0$ , with different strain parameter  $\varepsilon$  values of 0.025, 0.050, 0.075, and 0.100. We note that AGNRs have compressive edge stresses that tend to cause them to buckle.<sup>48-50</sup> Since a large unit cell of a buckled AGNR imposes a huge computational demand on accurate DFT calculations, we consider the AGNRs under tensile strain in this study.

The thermal conductance due to lattice vibrations  $K_{\text{ph}}$  is calculated according to

$$K_{\text{ph}}(\varepsilon, T) = \int_0^{\infty} h\nu \theta_{\text{ph}}(\nu) \frac{\partial n_{\text{B}}(\nu, T)}{\partial T} d\nu,$$

where  $n_{\text{B}}(\nu, T) = (e^{h\nu/kT} - 1)^{-1}$  is the Bose-Einstein distribution with frequency  $\nu$ , and  $\theta_{\text{ph}}(\nu)$  is the phonon transmission function obtained using the counting method on the phonon dispersion relations. The supercell force-constant method is used to perform the phonon calculations.<sup>39,51,52</sup>

## III. RESULTS AND DISCUSSION

We first examine the effect of tensile strain on the electronic band structures of the AGNR- $N$ . The electronic

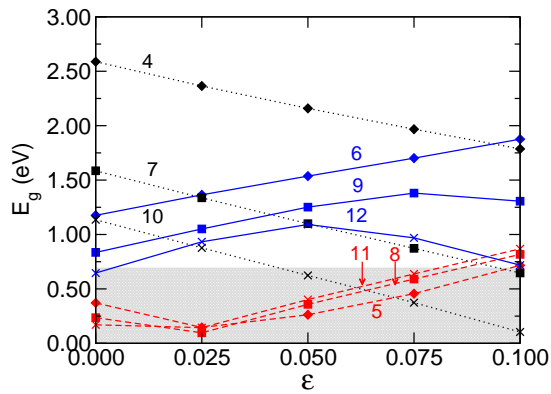


FIG. 2: Electronic band gap  $E_g$  versus strain parameter  $\varepsilon$  for AGNR- $N$ . The numbers within the graph represent  $N$ . The  $N = 3p + 1$ ,  $N = 3p$ , and  $N = 3p + 2$  families are represented by dotted lines (black), solid lines (blue), and dashed lines (red), respectively. The grey region indicates  $E_g < 10kT$  for  $T = 800$  K, where bipolar transport is important.

band gap  $E_g$  has a very important influence on the thermoelectric behavior of materials: we need an  $E_g$  of at least  $6kT$  to  $10kT$  to prevent bipolar transport because concurrent electron and hole transport leads to an opposing effect that reduces the Seebeck coefficient. Figure 2 shows the band gap  $E_g(\varepsilon)$  of the AGNRs as a function of  $\varepsilon$ . It is well-known that the use of the local density approximation for the exchange-correlation functional underestimates  $E_g$ , but we expect the correct overall qualitative trends to be obtained.<sup>53</sup> In our calculations using LDA,  $E_g$  ranges from 2.59 eV for AGNR-4 to 0.65 eV for AGNR-12. In comparison, with GW calculations,  $E_g$  varies from 5.56 eV for AGNR-4 to 1.67 eV for AGNR-12.<sup>53</sup> The  $E_g$  of AGNR- $N$  for  $\varepsilon = 0.00$  depends on  $N$  through a 3-family behavior:  $E_g(N = 3p + 1) > E_g(N = 3p) > E_g(N = 3p + 2)$ , where  $p$  is an integer.<sup>54</sup> Figure 2 shows how  $E_g$  varies with  $\varepsilon$  for different families. For the family with the largest  $E_g$ ,  $N = 3p + 1$ ,  $E_g$  decreases linearly with  $\varepsilon$ . For the family of  $N = 3p$ ,  $E_g$  increases with  $\varepsilon$  except for large  $\varepsilon$  for  $N = 9$  and 12. For the family of  $N = 3p + 2$ ,  $E_g$  generally increases with  $\varepsilon$  for all  $N$ , except at  $\varepsilon = 0.025$ . The maximum percentage change to  $E_g$  for  $\varepsilon = 0.0-0.1$  is substantial as it ranges from  $\sim -30\%$  in AGNR-4 to  $\sim +400\%$  in AGNR-11. For much wider AGNRs ( $N > 12$ ), a previous study<sup>55</sup> noted that  $E_g$  shows a zigzag fluctuation with  $\varepsilon$ . This suggests that it is much harder to tune  $E_g$  by modifying  $\varepsilon$  for large  $N$ .

The Lorenz functions in Eq. 4 for the evaluation of  $G_e$ ,  $|S|$ , and  $K_e$  depend critically on the location of  $\mu$  and the extent (or spread) of  $\frac{-\partial f}{\partial E}$ , both of which are controlled by the doping concentration and temperature. The values of  $\mu$  for AGNR-9 as a function of doping concentration for different  $\varepsilon$  are shown in Figure 3(c). The spread of  $\frac{-\partial f}{\partial E}$  spans only  $\sim 10kT$  around  $\mu$  (see Figure 3(d)), and thus severely restricts the range of  $E$  for the integration of  $L_n$ . As a reference, we note that at  $T = 800$  K,  $10kT$  corre-

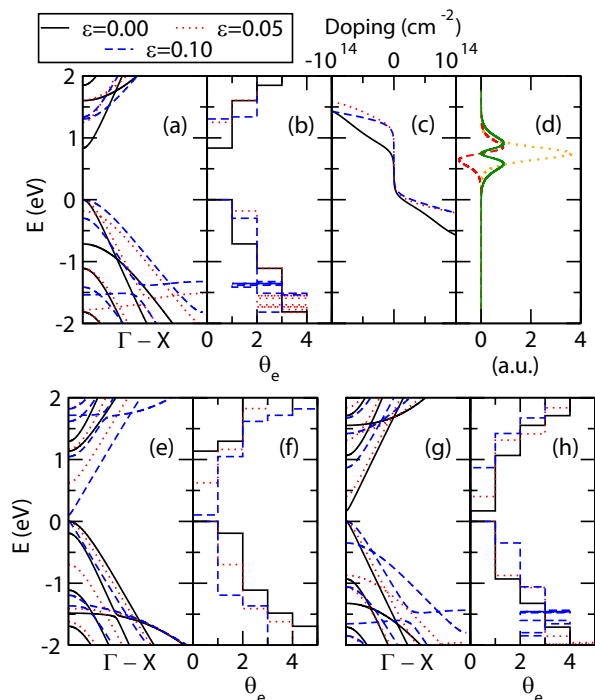


FIG. 3: The electronic band structure and corresponding  $\theta_e(E)$  of AGNR-9 (a, b), AGNR-10 (e, f), and AGNR-11 (g, h). (c) shows the variation of  $\mu$  for AGNR-9 with doping concentration (negative concentration represents n-type doping) at  $T = 800$  K. (d) shows the values of  $-(E - \mu)^n \frac{\partial f}{\partial E}$  as a function of  $E$  for  $n = 0$  (dotted orange line),  $n = 1$  (dashed red line), and  $n = 2$  (solid green line), for the determination of  $L_n$ . The  $\mu$  is chosen such that it maximizes  $ZT$  for AGNR-9 under n-type doping at  $T = 800$  K and  $\varepsilon = 0.00$ . The valence band maximum is set to 0 eV in all figures.

sponds to 0.69 eV. We shall therefore study the changes of  $\theta_e(E)$  around the conduction (valence) band edge induced by  $\varepsilon$  for n-type (p-type) doping to obtain a qualitative understanding of the variations of  $|S|$ ,  $G_e$ , and  $K_e$  as a result of  $\varepsilon$  and temperature.

Figure 3(a, e, g) shows the electronic band structures, and 3(b, f, h) the  $\theta_e(E)$  of the representative AGNR- $N$  from each family,  $N = 9, 10$ , and 11. From Figure 3(a), we observe that AGNR-9 from the  $N = 3p$  family displays an increase in  $\theta_e(E)$  near the band edges for non-zero  $\varepsilon$ . From Figure 3(f), AGNR-10 (a member of the  $N = 3p + 1$  family) shows a decrease in  $\theta_e(E)$  around the band edges. Finally, members of the  $N = 3p + 2$  family display very little changes in  $\theta_e(E)$  to within  $\sim 0.69$  eV (the range at which  $\frac{-\partial f}{\partial E}$  is nonzero at 800 K) around the band edges with increasing  $\varepsilon$ ; this is shown in Figure 3(h) for AGNR-11.

We plot the various transport parameters for the determination of  $ZT$  for n- and p-type doping in Figure 4 at 300 and 800 K with corresponding  $kT$  values of 0.026 and 0.069 eV, respectively. At a moderate temperature such as 300 K, the transport is governed by monopolar transport, where the values of  $G_e$ ,  $|S|$ , and  $K_e$  vary

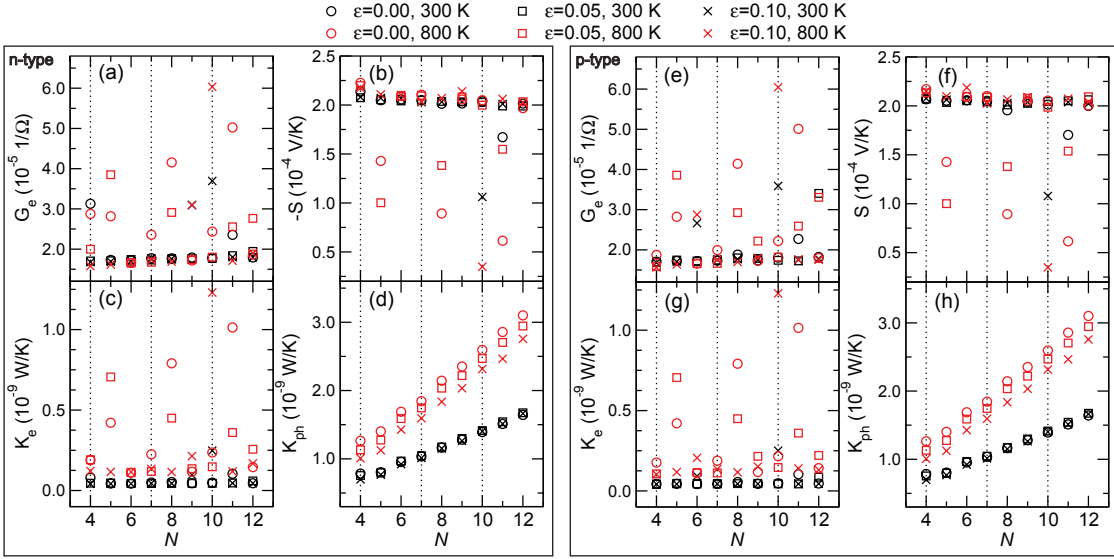


FIG. 4: Values of  $G_e$ ,  $|S|$ ,  $K_e$ , and  $K_{ph}$  for  $\epsilon = 0.00, 0.05$ , and  $0.10$  at  $T = 300$  and  $800$  K. n-type [(a) to (d)] doped and p-type [(e) to (h)] doped AGNRs are considered.  $\mu$  are chosen to maximize the  $ZT$  values. The vertical dotted grey lines identify the AGNRs belonging to the  $N = 3p + 1$  family.

only slightly with changes with  $\epsilon$ . Physically this means electronic excitation is limited at this temperature. The only exception is AGNR-10 at  $\epsilon = 0.100$ , where its  $E_g$  is so small compared to  $10kT$  that bipolar transport governs and causes drastic changes in  $G_e$ ,  $|S|$ , and  $K_e$ . At a high temperature  $T = 800$  K, we expect AGNR- $N$  with  $E_g \leq 10kT = 0.69$  eV to be affected by bipolar transport, where  $G_e$  and  $K_e$  will generally increase due to the presence of both types of carriers (i.e., electrons and holes) for charge and heat transport, but  $|S|$  will decrease due to the opposing effect we mentioned earlier. This is generally evident in Figure 4 where the values of  $G_e$ ,  $|S|$ , and  $K_e$  change drastically at  $T = 800$  K compared to that for  $T = 300$  K for all strain values, as long as  $E_g(\epsilon) \leq 0.69$  eV.

We shall give a detailed discussion of the effect of strain on AGNR- $N$ , first with  $N = 3p + 1$ , then  $N = 3p$ , and finally  $N = 3p + 2$ . Particular attention will be paid to the  $E_g$  variation in comparison with  $10kT$  as well as the changes in the  $\theta_e(E)$  due to  $\epsilon$  in determining the values of  $G_e$ ,  $|S|$ ,  $K_e$ ,  $K_{ph}$ , and finally  $ZT$ . Unless otherwise stated, the temperature is taken to be  $800$  K for the discussion. For AGNR- $N$  with  $N = 3p + 1$ ,  $G_e$  and  $K_e$  values decrease with increasing  $\epsilon$  for  $N = 4$  and  $7$  (due mainly to the reduction in  $\theta_e(E)$ ), but  $G_e$  and  $K_e$  increase with increasing  $\epsilon$  due to bipolar transport for  $N = 10$ . For  $|S|$ , it remains essentially constant for  $N = 4$  and  $7$ , but it decreases for  $N = 10$ . We note that  $|S|$  remains essentially constant for  $N = 4$  and  $7$  since it is proportional to  $L_1/L_0$ , so the changes in  $\theta_e(E)$  is somewhat suppressed when the ratio is taken. The net outcome for changes in  $G_e$ ,  $|S|$ , and  $K_e$ , is shown in Fig. 5(e) where the  $ZT$  value for AGNR- $(3p + 1)$  decreases with increasing  $\epsilon$ .

Next we discuss the  $N = 3p$  family, where  $\theta_e(E)$  and

$E_g$  of AGNRs in the  $N = 3p$  family generally increases with increasing  $\epsilon$ . The increase in  $\theta_e(E)$  causes  $G_e$ ,  $K_e$ , and  $|S|$  to increase with  $\epsilon$ . However, an increase in  $E_g(\epsilon)$  does not significantly benefit  $|S|$  because even the smallest  $E_g$  at  $\epsilon = 0.00$  for all AGNR- $3p$  is already large enough to prevent bipolar transport. Overall, at  $T = 800$  K, the increase in both  $G_e$  and  $K_e$  causes  $ZT$  to increase with strain  $\epsilon$  (see Fig. 5(e)).

Since AGNR- $(3p + 2)$  have the smallest  $E_g$  among the three families, therefore bipolar transport is present even at  $\epsilon = 0.00$  that benefits  $G_e$  and  $K_e$  but not  $|S|$ . At  $T = 800$  K, bipolar transport becomes dominant and causes  $|S|$  to become small. As  $E_g$  increases with increasing  $\epsilon$ ,  $G_e$  and  $K_e$  decrease but  $|S|$  increases since the monopolar transport becomes more pronounced. The overall effect, however, is to increase  $ZT$  as shown in Fig. 5(e).

We now examine the effect of  $\epsilon$  and temperature on  $K_{ph}$  and its associated influence on  $ZT$  of AGNRs. The effect of temperature is also seen (see Fig. 4(d)) to increase the thermal conductance due to phonon ( $K_{ph}$ ) from  $300$  K to  $800$  K. However, at high temperatures, the effect of strain on  $K_{ph}$  for various  $\epsilon$  could decrease the  $K_{ph}$  due an overall shifting down of the phonon frequencies as a result of weaker interatomic interactions.<sup>39</sup> For example, at  $T = 800$  K, a strain of  $\epsilon = 0.10$  could decrease  $K_{ph}$  by  $\sim 15\%$  from that of the unstrained AGNRs. We note that the total thermal conductance of AGNRs is dominated by  $K_{ph}$  and not  $K_e$ .

Figure 5 shows the maximum  $ZT$  values attainable at  $T = 300, 500$ , and  $800$  K for n- and p-type doping. It can be seen that at higher temperatures,  $ZT$  changes more sensitively with  $\epsilon$  because the larger spread of  $\frac{\partial f}{\partial E}$  magnifies the changes to  $\theta_e$  and  $E_g$  due to  $\epsilon$ . In general the  $ZT$  value decreases with increasing  $N$  due to the

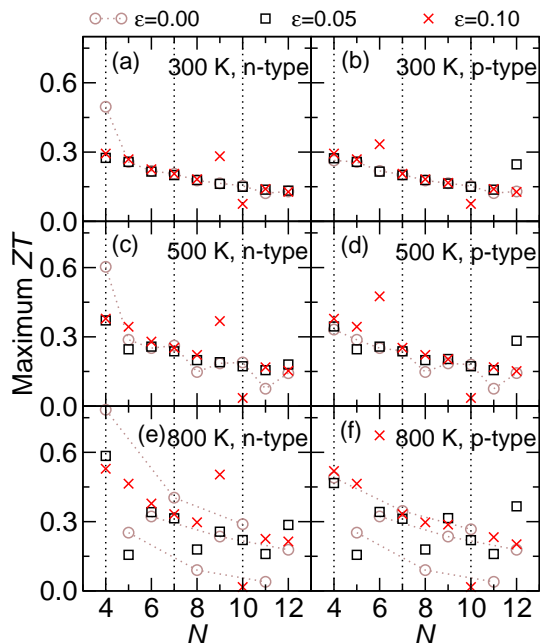


FIG. 5: Maximum  $ZT$  attainable at  $T = 300, 500,$  and  $800$  K for n- and p-type doping for  $\epsilon = 0.00, 0.05$  and  $0.10$ . The data for  $\epsilon = 0.00$  at  $800$  K is split into 3 sets to illustrate the 3-family behavior. The vertical dotted grey lines identify the AGNRs belonging to the  $N = 3p + 1$  family.

faster increase in  $K_{ph}$  as the AGNR- $N$  become wider. We observe that, under strain,  $ZT$  increases for AGNR- $N$  belonging to the  $N = 3p$  and  $N = 3p + 2$  families, but decreases for the  $N = 3p + 1$  family. It is interesting to note that at  $T = 800$  K and  $\epsilon = 0.00$ , bipolar transport becomes significant for AGNRs with small  $E_g$  such that the monotonic decrease in  $ZT$  values can be grouped according to three families, which is largely due to the 3-family behavior<sup>54</sup> exhibited by  $E_g$ .

Figure 6 shows the maximum  $ZT$  value attainable for AGNR- $N$  in the temperature range  $T = 200 - 800$  K and doping concentration of  $-10^{14}$  to  $10^{14}$   $\text{cm}^{-2}$ , giving an upper limit to the  $ZT$  value that can be achieved through strain engineering. At the highest  $\epsilon = 0.10$ ,  $ZT$  increases by 13.3 – 114.3% for AGNRs in the  $N = 3p$  family, and increases by 60.3 – 65.5% for the  $N = 3p + 2$  family. However,  $ZT$  decreases by 3.9 – 59.1% for the  $N = 3p + 1$  family.

## IV. CONCLUSION

We have calculated the thermoelectric figure of merit  $ZT$  for AGNR- $N$  ( $N$  is the number of carbon dimer lines across the AGNR width) when uniaxial tensile strain is applied along the main ribbon axis of the AGNR. We have considered both n- and p-type doping concentrations of up to  $10^{14}$   $\text{cm}^{-2}$  and a temperature range of 200–800 K. Using density-functional theory calculations,

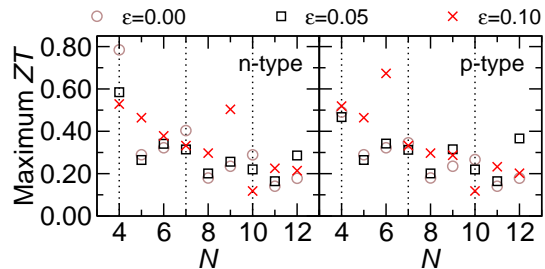


FIG. 6: Maximum attainable  $ZT$  for AGNR- $N$  in the temperature range of 200 to 800 K and doping concentration range of  $-10^{14}$  to  $10^{14}$   $\text{cm}^{-2}$ . For  $\epsilon = 0.10$ , AGNR-9 and AGNR-6 have the largest  $ZT$  values under n-type and p-type doping, respectively. For AGNR-9 the maximum  $ZT$  of 0.504 is achieved at  $T = 800$  K and a doping concentration of  $-1.64 \times 10^{12}$   $\text{cm}^{-2}$ ; for AGNR-6, the maximum  $ZT$  of 0.673 is achieved at  $T = 800$  K and a doping concentration of  $3.30 \times 10^{13}$   $\text{cm}^{-2}$ .

the effect of  $\epsilon$  is found to improve  $ZT$  for AGNR- $N$ , for  $N = 3p$  and  $N = 3p + 2$ . For the  $N = 3p$  family, this is due to an increase in the electronic transmission around the valence and conduction band edges. For the  $N = 3p + 2$  family, it is due to an increase in the band gap that reduces the unfavorable bipolar transport. Based on first principles, we concluded that strain engineering provides a possible route to improve the  $ZT$  values of two families of AGNR- $N$ .

## Acknowledgements

We gratefully acknowledge the support of A\*STAR Computational Resource Center (A\*CRC) of Singapore.

\* Electronic address: ganck@ihpc.a-star.edu.sg

<sup>1</sup> J. R. Szczech, J. M. Higgins, and S. Jin, *J. Mater. Chem.* **21**, 4037 (2011).

<sup>2</sup> G. J. Snyder and E. S. Toberer, *Nat. Mater.* **7**, 105 (2008).

<sup>3</sup> J. R. Sootsman, D. Y. Chung, and M. G. Kanatzidis, *Angewandte Chemie International Edition* **48**, 8616 (2009).

<sup>4</sup> T. M. Tritt, *Annu. Rev. Mater. Res.* **41**, 433 (2011).

<sup>5</sup> D. Teweldebrhan, V. Goyal, M. Rahman, and A. A. Ba-

landin, *Applied Physics Letters* **96**, 053107 (2010), ISSN 00036951.

<sup>6</sup> V. Goyal, D. Teweldebrhan, and A. A. Balandin, *Applied Physics Letters* **97**, 133117 (2010), ISSN 00036951.

<sup>7</sup> D. Teweldebrhan, V. Goyal, and A. A. Balandin, *Nano Letters* **10**, 1209 (2010), ISSN 1530-6984.

<sup>8</sup> K. I. Bolotin, K. J. Sikes, J. Hone, H. L. Stormer, and P. Kim, *Phys. Rev. Lett.* **101**, 096802 (2008).

- <sup>9</sup> Y. M. Zuev, W. Chang, and P. Kim, *Phys. Rev. Lett.* **102**, 096807 (2009).
- <sup>10</sup> P. Wei, W. Bao, Y. Pu, C. N. Lau, and J. Shi, *Phys. Rev. Lett.* **102**, 166808 (2009).
- <sup>11</sup> J. G. Checkelsky and N. P. Ong, *Phys. Rev. B* **80**, 081413 (2009).
- <sup>12</sup> T. C. Harman, P. J. Taylor, M. P. Walsh, and B. E. LaForge, *Science* **297**, 2229 (2002).
- <sup>13</sup> K. F. Hsu, S. Loo, F. Guo, W. Chen, J. S. Dyck, C. Uher, T. Hogan, E. K. Polychroniadis, and M. G. Kanatzidis, *Science* **303**, 818 (2004).
- <sup>14</sup> H. Ohta, S. Kim, Y. Mune, T. Mizoguchi, K. Nomura, S. Ohta, T. Nomura, Y. Nakanishi, Y. Ikuhara, M. Hirano, et al., *Nature Mater.* **6**, 129 (2007).
- <sup>15</sup> N. Dubey and M. Leclerc, *J. Polym. Sci., Part B: Polym. Phys.* **49**, 467 (2011).
- <sup>16</sup> A. A. Balandin, S. Ghosh, W. Bao, I. Calizo, D. Teweldebrhan, F. Miao, and C. N. Lau, *Nano Lett.* **8**, 902 (2008).
- <sup>17</sup> C. Faugeras, B. Faugeras, M. Orlita, M. Potemski, R. R. Nair, and A. K. Geim, *ACS Nano* **4**, 1889 (2010).
- <sup>18</sup> A. A. Balandin, *Nature Mater.* **10**, 569 (2011).
- <sup>19</sup> D. L. Nika and A. A. Balandin, *Journal of Physics: Condensed Matter* **24**, 233203 (2012), ISSN 0953-8984.
- <sup>20</sup> Y. Ouyang and J. Guo, *Appl. Phys. Lett.* **94**, 263107 (2009).
- <sup>21</sup> F. Mazzamuto, J. Saint-Martin, V. H. Nguyen, C. Chassat, and P. Dollfus, *J. Comput. Chem. Electron.* **11**, 67 (2012).
- <sup>22</sup> H. Sevinçli and G. Cuniberti, *Phys. Rev. B* **81**, 113401 (2010).
- <sup>23</sup> T. Gunst, T. Markussen, A. -P. Jauho, and M. Brandbyge, *Phys. Rev. B* **84**, 155449 (2011).
- <sup>24</sup> W. Zhao, Z. X. Guo, J. X. Cao, and J. W. Ding, *AIP Advances* **1**, 042135 (2011).
- <sup>25</sup> Y. Chen, T. Jayasekera, A. Calzolari, K. W. Kim, and M. Buongiorno Nardelli, *J. Phys.: Condens. Matter* **22**, 372202 (2010).
- <sup>26</sup> Z.-X. Xie, L.-M. Tang, C.-N. Pan, K.-M. Li, K.-Q. Chen, and W. Duan, *Appl. Phys. Lett.* **100**, 073105 (2012).
- <sup>27</sup> W. Huang, J.-S. Wang, and G. Liang, *Phys. Rev. B* **84**, 045410 (2011).
- <sup>28</sup> L. Liang, E. Cruz-Silva, E. C. Girão, and V. Meunier, *Phys. Rev. B* **86**, 115438 (2012).
- <sup>29</sup> F. Mazzamuto, V. Hung Nguyen, Y. Apertet, C. Caër, C. Chassat, J. Saint-Martin, and P. Dollfus, *Phys. Rev. B* **83**, 235426 (2011).
- <sup>30</sup> P.-H. Chang and B. K. Nikolić, *Phys. Rev. B* **86**, 041406 (2012).
- <sup>31</sup> X. Ni, G. Liang, J.-S. Wang, and B. Li, *Appl. Phys. Lett.* **95**, 192114 (2009).
- <sup>32</sup> K. Yang, Y. Chen, R. D'Agosta, Y. Xie, J. Zhong, and A. Rubio, *Phys. Rev. B* **86**, 045425 (2012).
- <sup>33</sup> S. Chen, Q. Wu, C. Mishra, J. Kang, H. Zhang, K. Cho, W. Cai, A. A. Balandin, and R. S. Ruoff, *Nature Materials* **11**, 203 (2012), ISSN 1476-1122.
- <sup>34</sup> A. A. Balandin and D. L. Nika, *Materials Today* **15**, 266 (2012), ISSN 1369-7021.
- <sup>35</sup> D. C. Elias, R. R. Nair, T. M. G. Mohiuddin, S. V. Morozov, P. Blake, M. P. Halsall, A. C. Ferrari, D. W. Boukhvalov, M. I. Katsnelson, A. K. Geim, et al., *Science* **323**, 610 (2009).
- <sup>36</sup> L. Ci, L. Song, C. Jin, D. Jariwala, D. Wu, Y. Li, A. Srivastava, Z. F. Wang, K. Storr, L. Balicas, et al., *Nat. Mater.* **9**, 430 (2010).
- <sup>37</sup> X. Zhai and G. Jin, *EPL (Europhysics Letters)* **96**, 16002 (2011).
- <sup>38</sup> N. Wei, L. Xu, H. Q. Wang, and J. C. Zheng, *Nanotechnology* **22**, 105705 (2011).
- <sup>39</sup> P. S. E. Yeo, K. P. Loh, and C. K. Gan, *Nanotechnology* **23**, 495702 (2012).
- <sup>40</sup> T.-Y. Lu, X.-X. Liao, H.-Q. Wang, and J.-C. Zheng, *J. Mater. Chem.* **22**, 10062 (2012).
- <sup>41</sup> K. I. Bolotin, K. J. Sikes, Z. Jiang, M. Klima, G. Fudenberg, J. Hone, P. Kim, and H. L. Stormer, *Solid State Commun.* **146**, 351 (2008).
- <sup>42</sup> S. Ghosh, I. Calizo, D. Teweldebrhan, E. P. Pokatilov, D. L. Nika, A. A. Balandin, W. Bao, F. Miao, and C. N. Lau, *Appl. Phys. Lett.* **92**, 151911 (2008).
- <sup>43</sup> T. Markussen, A. -P. Jauho, and M. Brandbyge, *Nano Lett.* **8**, 3771 (2008).
- <sup>44</sup> C. Jeong, R. Kim, M. Luisier, S. Datta, and M. Lundstrom, *J. Appl. Phys.* **107**, 023707 (2010).
- <sup>45</sup> J.-S. Wang, B. K. Agarwalla, H. Li, and J. Thingna, *Frontiers of Physics* p. 1 (2013).
- <sup>46</sup> B. Lee, Y. Chen, F. Duerr, D. Mastrogianni, E. Garfunkel, E. Y. Andrei, and V. Podzorov, *Nano Lett.* **10**, 2427 (2010).
- <sup>47</sup> J. Soler, E. Artacho, J. D. Gale, A. García, J. Junquera, P. Ordejón, and D. Sánchez-Portal, *J. Phys.: Condens. Matter* **14**, 2745 (2002).
- <sup>48</sup> C. K. Gan and D. J. Srolovitz, *Phys. Rev. B* **81**, 125445 (2010).
- <sup>49</sup> W. Bao, F. Miao, Z. Chen, H. Zhang, W. Jang, C. Dames, and C. N. Lau, *Nature Nanotech.* **4**, 562 (2009).
- <sup>50</sup> S. Kumar, K. P. S. S. Hembram, and U. V. Waghmare, *Phys. Rev. B* **82**, 115411 (2010).
- <sup>51</sup> C. K. Gan, Y. P. Feng, and D. J. Srolovitz, *Phys. Rev. B* **73**, 235214 (2006).
- <sup>52</sup> Y. Y. Zhao, K. T. E. Chua, C. K. Gan, J. Zhang, B. Peng, Z. P. Peng, and Q. H. Xiong, *Phys. Rev. B* **84**, 205330 (2011).
- <sup>53</sup> L. Yang, C.-H. Park, Y.-W. Son, M. L. Cohen, and S. G. Louie, *Physical Review Letters* **99**, 186801 (2007).
- <sup>54</sup> Y. W. Son, M. L. Cohen, and S. G. Louie, *Phys. Rev. Lett.* **97**, 216803 (2006).
- <sup>55</sup> L. Sun, Q. Li, H. Ren, H. Su, Q. W. Shi, and J. Yang, *J. Chem. Phys.* **129**, 074704 (2008).